Struct Chem (2014) 25:649–657
DOI 10.1007/s11224-013-0367-1

ORIGINAL RESEARCH

Redox interactions between structurally different alkylresorcinols and iron(III) in aqueous media: frozen-solution ^{57}Fe Mössbauer spectroscopic studies, redox kinetics and quantum chemical evaluation of the alkylresorcinol reactivities

Alexander A. Kamnev · Roman L. Dykman · Krisztina Kovács · Alexei N. Pankratov · Anna V. Tugarova · Zoltán Homonnay · Ernő Kuzmann

Received: 3 October 2013 / Accepted: 24 October 2013 / Published online: 8 November 2013

Abstract Iron(III)-containing aqueous solutions of 5-methylresorcinol (5-MR), 5-*n*-propylresorcinol (5-*n*-PR) and 4-*n*-hexylresorcinol (4-*n*-HR) at pH $\sim$ 3 were studied by means of ^{57}Fe transmission Mössbauer spectroscopy. Kinetic considerations were applied to the redox reactions. Density Functional Theory (DFT) calculations were performed for the alkylresorcinol (AR) molecules and their non-alkylated analogue (resorcinol). Mössbauer spectra consisted of quadrupole doublets assigned to high-spin Fe(III) and Fe(II) species. From changes in their relative spectral areas, a gradual reduction of Fe(III) by all the ARs studied was observed. However, significant differences were found for the reduction rates among the ARs. The following series of the reduction rates was established by means of Mössbauer spectroscopy: 4-*n*-HR $\gg$ 5-MR $>$ 5-*n*-PR, supplemented by rate constants calculated using a kinetic model. DFT calculations resulted in the following series: 4-*n*-HR $\gg$ 5-*n*-PR $>$ 5-MR $\gg$ resorcinol (the latter is not oxidised under the conditions applied). The reversed order of the experimentally observed 5-MR and 5-*n*-PR oxidation rates may be explained in terms of their different kinetic parameters related to their structure.

A. A. Kamnev (✉) · R. L. Dykman · A. V. Tugarova
Laboratory of Biochemistry, Institute of Biochemistry and Physiology of Plants and Microorganisms, Russian Academy of Sciences, 13 Prospekt Entuziastov, 410049 Saratov, Russia
e-mail: a.a.kamnev@mail.ru; aakamnev@ibppm.sgu.ru

K. Kovács · Z. Homonnay · E. Kuzmann
Laboratory of Nuclear Chemistry, Institute of Chemistry, Eötvös Loránd University, P.O. Box 32, Budapest 1512, Hungary

A. N. Pankratov
Division of Analytical Chemistry and Chemical Ecology, Institute of Chemistry, N.G. Chernyshevskii Saratov State University, 83 Astrakhanskaya Street, 410012 Saratov, Russia

Keywords Alkylresorcinols · Iron(III) reduction · Frozen-solution ^{57}Fe transmission Mössbauer spectroscopy · Redox kinetics · DFT calculations

Introduction

The ability of microbial cells to synthesize, excrete and use relatively small biomolecules as a 'chemical language' for communicating in consortia, discerning the population density ('quorum sensing') and coordinating their 'concerted activities' has been well-documented and generally accepted [1–4]. Knowledge of the physical chemistry, structural specificity and reactivity of such extracellular signalling molecules is of paramount importance for understanding and predicting abiotic effects of the environmental conditions on microbial communication [5, 6]. Any possible chemical transformations of such molecular signals (e.g. hydrolysis, complexation or oxidation reactions) in the surrounding medium, such as soil, would result in their evident exclusion from the signalling pathways, which is equivalent to a 'message non-delivery' [6]. However, while there has been extensive literature concerning a diversity of biological aspects of various signalling processes, the 'chemical fate' of the extracellularly excreted substances involved in microbial communication has so far received incomparably less attention, being virtually underestimated [5–7].

In a series of our earlier reports, it was shown that some relatively simple biological molecules involved in microbial intercellular signalling or metabolic pathways could be oxidised in the presence of iron(III), particularly in weakly acidic aqueous media [8–12]. Under similar conditions, the oxidation rates of such molecules typically depend on their structure, as was well illustrated using the example of

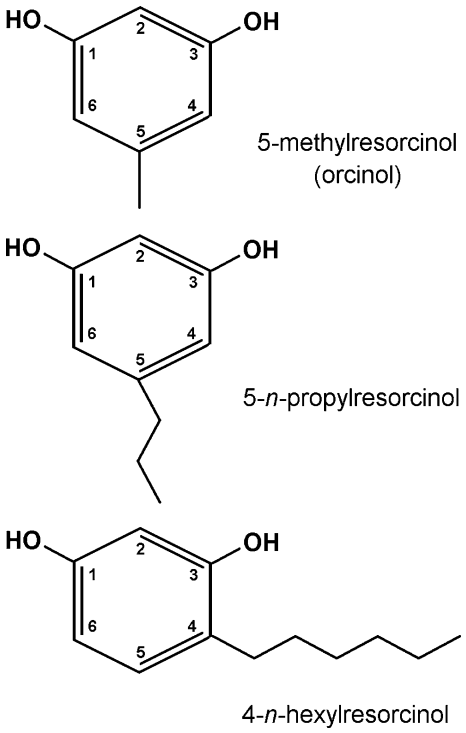

Fig. 1 Schematic representation of the structures of alkylresorcinols under study: 5-methylresorcinol (orcinol), 5-*n*-propylresorcinol and 4-*n*-hexylresorcinol (the *numeration* of carbon atoms in the aromatic ring is also shown)

various indole-3-alkanoic acids (auxin phytohormones, many of which are produced by soil bacteria; [10]). Fe, which in aerobic conditions is mainly represented by Fe(III) species, is ubiquitous in soils and aquifers. Moreover, acidic environments, including soils, are relatively widespread both in wild nature and among arable territories [13, 14]. In addition, local acidification of the medium is possible as a result of microbial and plant-root metabolic activities [15, 16].

Alkylresorcinols (*ARs*; 1,3-dihydroxybenzenes with alkyl substituents in positions 4 or 5), representing a separate specific subclass of alkylated hydroxybenzenes (phenols), comprise a group of natural substances with a wide range of known biological functions [17–20]. In particular, ARs with varying alkyl chain lengths are used by many microorganisms as extracellular autoinducers with adaptogenic functions under unfavourable conditions [18, 19, 21–23]. They also have antioxidant and antiradical activities [24].

The goal of this work was to quantitatively assess and compare the reactivities of ARs with different structures (in terms of the length and position of the alkyl substituent; Fig. 1): 5-methylresorcinol (5-MR), 5-*n*-propylresorcinol (5-*n*-PR) and 4-*n*-hexylresorcinol (4-*n*-HR). Redox reactions involving each of the three ARs were studied in Fe(III)-containing moderately acidic aqueous media by means of frozen-solution ^{57}Fe transmission Mössbauer spectroscopy [25–27]. A kinetic scheme of the redox interactions is proposed and verified using the Mössbauer spectroscopic data obtained. In an attempt to explain the relative reactivities of the three ARs under study, quantum chemical calculations were also performed (involving also the non-alkylated analogue, resorcinol, which is less reactive under similar conditions [7]).

Materials and methods

Materials

The main organic chemicals used were: 5-MR (orcinol, also known as orcine, 1,3-dihydroxy-5-methylbenzene) monohydrate ($C_7H_8O_2{\cdot}H_2O$, obtained from 'Fluka', No. 75420), 5-*n*-PR, $C_9H_{12}O_2$ (1,3-dihydroxy-5-*n*-propylbenzene, obtained from 'Enamine', Kiev, Ukraine; http://www.enamine.net/), as well as 4-*n*-HR (1,3-dihydroxy-4-*n*-hexylbenzene, $C_{12}H_{18}O_2$, 'Sigma', No. 209465). All the substances were of the 'chemical purity' grade and used as received; their structural formulas are schematically shown in Fig. 1.

Fe(III) for preparing samples for Mössbauer measurements was used in this work as a 0.1 M aqueous stock solution of $FeCl_3$ (90 % enriched with ^{57}Fe in order to increase the Mössbauer effect in frozen solutions). The reaction mixtures contained 0.50 mL of initial 0.06 M aqueous solution of an AR (in case of 4-*n*-HR, its aqueous solution with 25 vol.% of absolute ethanol was used in order to increase its solubility; the final concentration of ethanol in all 4-*n*-HR samples was 20 vol.%; see below also for 5-MR) and 0.10 mL of 0.1 M aqueous solution of $^{57}FeCl_3$, corresponding to molar ratio Fe:AR = 1:3 (total concentration of Fe in each of the final mixtures was 0.016 M). Immediately before adding AR, the pH value of the solutions was adjusted to the required level (pH $\sim$ 3) by adding small amounts of 1 M KOH under constant stirring. The resulting reaction mixtures were stored at room temperature (296 $\pm$ 2 K) for specified periods of time in inert plastic sample holders (covered with foil to prevent any possible effects of light [28] and evaporation) and then frozen dropwisely in liquid nitrogen for Mössbauer measurements [25].

In order to check whether 20 vol.% of ethanol (necessarily added in case of 4-*n*-HR) exerts any appreciable influence on the reaction rate, for 5-MR (well soluble in water), a comparative experiment was performed, in addition to a sample in aqueous mixture, also using its mixture prepared as above with 20 vol.% ethanol (both samples were stored at room temperature for 3 h before freezing).

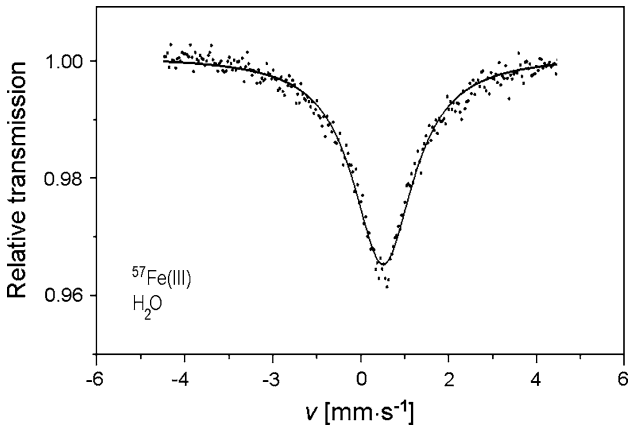

Fig. 2 Mössbauer spectrum of a frozen sample of the initial aqueous $^{57}FeCl_3$ solution (0.056 M) used for experiments on alkylresorcinol oxidation (measured at $T = 80$ K)

Mössbauer spectroscopic measurements

All Mössbauer spectroscopic measurements were performed in frozen solutions (at $T \sim 80$ K). Each frozen sample was placed in a specially designed 'cold-finger' cryostat filled with liquid nitrogen. For the initial $^{57}Fe^{III}$ solution, in order to confirm the absence of $^{57}Fe^{II}$, a Mössbauer spectrum was measured for a sample of its solution similarly diluted with water (0.056 M $^{57}Fe^{III}$; 0.6 mL) and frozen as mentioned above (Fig. 2).

Mössbauer spectra were recorded using a conventional constant acceleration Mössbauer spectrometer (WISSEL, FRG), coupled to a computer-operated multichannel analyser and a ^{57}Co(Rh) source (50 mCi) kept at room temperature. Evaluation of the spectra was performed using the MOSSWINN 3.0 programme [29]; all other methodological details had been described elsewhere [10–12]. The calculated parameters were the isomer shift (δ, mm s^{-1}, relative to α-Fe at room temperature), quadrupole splitting (Δ, mm s^{-1}), experimentally observed line width (full width at half maximum, W, mm s^{-1}) and partial resonant absorption area (A, %) for each spectral component. The latter parameter (A) is commonly used to represent the relative content of the corresponding Fe form (type of microenvironment), reasonably assuming equal recoilless fractions for all forms in a sample contributing to the spectrum at low temperature. In Mössbauer spectra, relative transmission of γ-radiation (in fractions of unity) was plotted against relative velocity (v, in mm s^{-1}) of the ^{57}Co(Rh) 14.4-keV γ-radiation source versus the absorber (a ^{57}Fe-containing sample), which corresponds to the energy scale according to the Doppler effect (i.e. with ±1 mm s^{-1} corresponding to ±48.1 neV; [26]), calibrated using α-Fe foil at room temperature.

Computational details

Quantum chemical computations were carried out by means of the hybrid Density Functional Theory (DFT) method [30–32] in the B3LYP variant [33–35] with the 6-311++G(3*d*,3*p*) basis set [36, 37] using the *Gaussian 03W* programme complex [38], analogously to the manner realised in the reports cited in [39]. The initial geometries were generated by means of the *HyperChem* software package (*HyperChem* [TM], Hypercube, Inc., 1115 NW 4th Street, Gainesville, Florida 32601, USA; [40]) and optimized by the PM3 method [41, 42].

Results and discussion

Mössbauer spectroscopy

The resulting Mössbauer spectra of the samples in frozen solutions are presented in Figs. 2 and 3. For the initial $^{57}Fe^{III}$ solution, the spectrum (Fig. 2) shows a typical broad line due to a slow paramagnetic spin relaxation (characteristic of monomeric Fe^{3+} ions; [25]). In this spectrum, no subspectra characteristic of Fe(II) [43] were observed. This confirms the absence of Fe(II) in the initial solution used for preparing mixtures with ARs.

As can be seen from Fig. 3, all the spectra of AR-containing samples can be decomposed into two quadrupole doublets. The corresponding Mössbauer parameters are given in Table 1.

In all the solutions, the Mössbauer parameters for Fe(II), which appeared as a result of Fe(III) reduction by the ARs under study, featured by quadrupole doublets (depicted by dark shaded spectral components in Fig. 3), were within the following ranges: isomer shift, ~1.3–1.4 mm s^{-1}; quadrupole splitting, ~3.2–3.4 mm s^{-1} (see Table 1). These values are characteristic of high-spin Fe^{2+} [43]. The Mössbauer parameters of Fe(II) microenvironments are typical for Fe^{2+} hexaaquo complexes [25]. Furthermore, some line broadening (linewidths, W, over 0.3–0.4 mm s^{-1}), as compared to that expected owing to the thickness effect [44], may indicate the presence of slightly different microenvironments in the system because of differences in possible coordination of AR oxidation products, evidently along with H_2O molecules.

For 5-MR solutions at pH ~ 3, an increase in the relative area of the Fe(II) quadrupole doublet was observed with time after mixing (Fig. 3a–d; Table 1). This reflects a gradual slow reduction of Fe(III) to Fe(II). Within the reaction time span from 10 min to 5.5 h, the fraction of reduced Fe(II) increased from ca. 6 to 26 % of the total Fe (see Table 1).

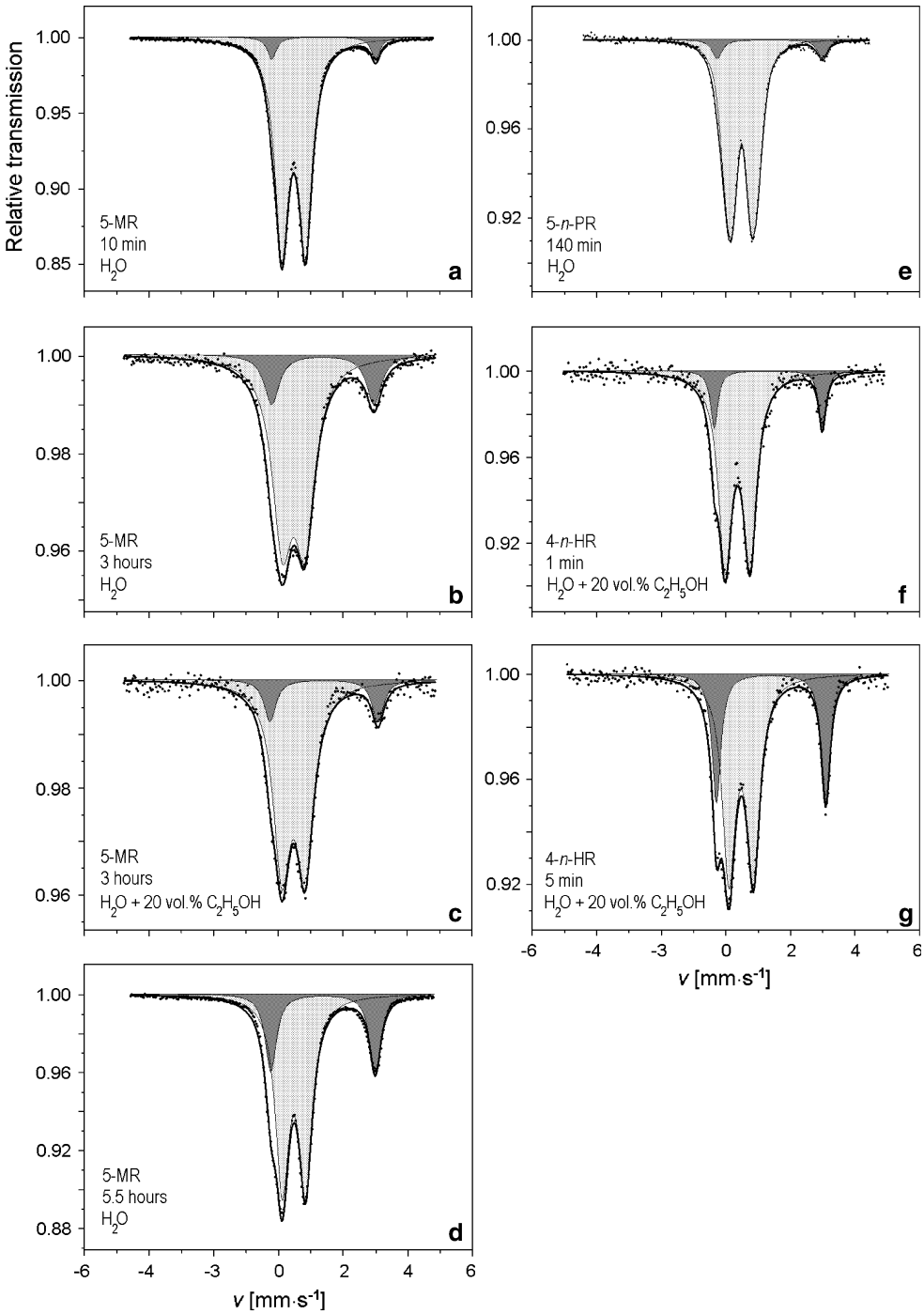

Fig. 3 Mössbauer spectra of the products of [^{57}Fe]-iron(III) interaction with 5-methylresorcinol (5-MR, **a**–**d**), 5-*n*-propylresorcinol (5-*n*-PR, **e**) and 4-*n*-hexylresorcinol (4-*n*-HR, **f**, **g**) in aqueous solutions (**a**, **b**, **d**, **e**) or in the presence of 20 vol.% ethanol (**c**, **f**, **g**) at pH ~ 3 rapidly frozen in liquid nitrogen 10 min (**a**), 3 h (**b**, **c**), 5.5 h (**d**), 140 min (**e**), 1 min (**f**) or 5 min (**g**) after mixing the reagents (all spectra measured at $T = 80$ K). The *shaded areas* (quadrupole doublets) represent contributions of Fe^{III} (*lightly shaded areas*) or Fe^{II} (*dark shaded areas*) to the whole spectrum area (defined by the outer *solid-line* envelope) calculated by fitting the experimental data (*points*)

It has to be noted that, while 5-MR is very well soluble in water, similar experiments with 4-*n*-HR (see below) at its comparable concentrations could only be performed in aqueous solutions containing minimum 20 vol.% ethanol to increase its solubility. In order to check whether 20 vol.% of added ethanol could have any appreciable influence on the reaction rate, comparative experiments were performed with 5-MR in $^{57}Fe^{III}$-containing solutions both in water (Fig. 3b) and in the presence of 20 vol.% ethanol (Fig. 3c), each kept in the dark for 3 h at ambient temperature and then frozen for Mössbauer measurements. As can be seen from Table 1, in these cases the spectral area fractions of Fe(II) in aqueous solutions without and with ethanol reached ca. 18 and 14 %, respectively. This relatively small difference of a few percent can be assumed to originate from both the experimental errors of Mössbauer measurements and possible slight differences in the pH values. The Mössbauer parameters for these two frozen solutions of 5-MR without and with ethanol (see Table 1) are also closely matching. Thus, the presence of 20 vol.%

Table 1 Calculated Mössbauer parameters for $^{57}Fe^{III}$-containing aqueous solutions of 5-methylresorcinol (5-MR, orcinol, see also Fig. 2b–e), 5-*n*-propylresorcinol (5-*n*-PR, see also Fig. 2f) and 4-*n*-hexylresorcinol (4-*n*-HR, see also Fig. 2g, h) at pH ~ 3 (total [Fe] = 0.016 ± 0.001 M, Fe-to-AR molar ratios 1:3), rapidly frozen after specified periods of time (all spectra measured at $T = 80$ K)

Alkylresorcinol mixed with $^{57}Fe^{III}$ in solution	Time[a]	Fe oxidation state	δ[b] (mm s^{-1})	Δ[c] (mm s^{-1})	W[d] (mm s^{-1})	A[e] (%)
5-MR	10 min	+3	0.48 (1)	0.74 (1)	0.52 (1)	93.3
		+2	1.41 (1)	3.22 (1)	0.34 (1)	6.7
	3 h	+3	0.478 (3)	0.70 (1)	0.75 (1)	82.1
		+2	1.39 (1)	3.17 (1)	0.56 (2)	17.9
	3 h[f]	+3	0.475 (4)	0.72 (1)	0.64 (1)	86.2
		+2	1.42 (1)	3.34 (2)	0.44 (3)	13.8
	5.5 h	+3	0.48 (1)	0.72 (1)	0.50 (1)	74.1
		+2	1.38 (1)	3.23 (1)	0.42 (1)	25.9
5-*n*-PR	140 min	+3[g]	0.47 (1)	0.80 (2)	0.25 (2)	92.0
		+2	1.35 (1)	3.26 (1)	0.40 (2)	8.0
4-*n*-HR	1 min[f]	+3	0.4 (1)	0.77 (3)	0.51 (3)	85.6
		+2	1.31 (1)	3.35 (1)	0.27 (2)	14.4
	5 min[f]	+3	0.475 (3)	0.757 (4)	0.49 (1)	68.8
		+2	1.402 (3)	3.388 (5)	0.34 (1)	31.2

Calculated errors (SD, in the last digits) are given in parentheses

[a] Period from mixing the reagents until rapid freezing of the solution

[b] Isomer shift (relative to α-Fe at ambient temperature)

[c] Quadrupole splitting

[d] Full line width at half maximum

[e] Partial resonant absorption areas of spectral components which represent relative contents of the corresponding Fe forms assuming a common recoilless fraction for all forms (for A, relative error is ca. ±4 % of the given values)

[f] In aqueous solution containing 20 vol.% ethanol

[g] Fitted with a distribution of Δ owing to multiple similar Fe^{3+} microenvironments (average parameters are given)

ethanol may be regarded as having a virtually insignificant effect on the reaction rate and products.

In the case of 5-*n*-PR, 140 min after mixing, the Mössbauer spectrum (Fig. 3e) reveals a relatively small contribution (8 %) of Fe(II) quadrupole doublet as compared to the corresponding samples of 5-MR. This means, interestingly, that 5-*n*-PR shows a significantly slower reduction of Fe(III) than 5-MR at pH ~ 3.

In contrast, the Mössbauer spectra of 4-*n*-HR solutions (Fig. 3f, g) show relatively high contributions of Fe(II) quadrupole doublets already a few minutes after mixing (e.g. 31 % after 5 min; see Table 1). This reflects a remarkably higher redox reaction rate for 4-*n*-HR at pH ~ 3 than for the other ARs under study.

For all ARs solutions, the Mössbauer parameters of quadrupole doublets assigned to Fe(III), featured by slightly broadened lines, were found to be within the following ranges: isomer shift, 0.4–0.5 mm s^{-1}; quadrupole splitting, 0.7–0.8 mm s^{-1} (see Table 1). These parameters at ~80 K are typical for high-spin Fe(III) compounds [43] and fall within the range of those for hydrolysed polymeric (colloidal) species at pH ~ 3 [25]. The Fe(III) quadrupole doublet may be assigned to a microenvironment such as $[Fe^{III}_x(OH)_y]^{3x-y}$ (without considering water molecules which can also be coordinated; see 'Kinetic considerations' section below). The Mössbauer parameters seem to be insensitive to the occurrence of AR oxidation products in the vicinity of hydrolysed Fe(III) species.

Thus, the Mössbauer experimental data showed a gradual reduction of Fe(III) at pH ~ 3 by the ARs studied. However, significant differences were found for the reduction rates between the ARs. The following series of the reduction rates was established by means of Mössbauer spectroscopy: 4-*n*-HR ≫ 5-MR > 5-*n*-PR.

Kinetic considerations

According to the literature [17, 18, 45], the first step of AR oxidation is commonly an additional hydroxylation of the benzene ring with the formation of trihydroxylated alkylbenzenes. This is formally equivalent to the introduction of an oxygen atom into a C–H bond in the aromatic ring with the formation of the corresponding C–O–H bond:

$$AlkC_6H_3(OH)_2 + [O] = AlkC_6H_2(OH)_3, \quad (1)$$

where Alk denotes an alkyl group.

Under the conditions applied (pH ~ 3), as mentioned above, Fe(III) is typically found in the form of colloidal (polymeric) hydrolysed species. Thus, considering that the first step of AR oxidation is a two-electron reaction (requiring two Fe^{3+} ions to be reduced to Fe^{2+}), the reaction between Fe(III) and an AR under these conditions may be considered to take place between a couple of adjacent hydroxylated Fe^{3+} ions in a polymeric species and an AR molecule according to the following general scheme (not showing the hydration of ions common for aqueous solutions):

$$\left[Fe_2^{III}(OH)_2\right]^{4+} + AlkC_6H_3(OH)_2 = 2Fe^{2+} + H_2O + AlkC_6H_2(OH)_3, \quad (2)$$

or a more general scheme involving a polynuclear Fe(III) hydroxylated species:

$$\left[Fe_x^{III}(OH)_y\right]^{3x-y} + AlkC_6H_3(OH)_2 = 2Fe^{2+} + \left[Fe_{x-2}^{III}(OH)_{y-2}\right]^{3x-y-4} + H_2O + AlkC_6H_2(OH)_3. \quad (3)$$

According to this scheme, the reaction rate should be expected to be proportional to the overall Fe(III) concentration and to the AR concentration. In our experiments, the initial [Fe^{3+}]-to-[AR] molar ratio was taken to be 1:3 in all cases, and the range of total Fe(III) fraction reduced to Fe(II) was within 6.7–31.2 % (see Table 1). Since 2 mol of Fe(III) reduced to Fe(II) correspond to one mole of oxidised AR (see Schemes (2), (3)), the overall fraction of AR oxidised in our experiments is expected to be within ~1.1–5.2 % (thus, it generally did not exceed ca. 5 %). In this case, for kinetic calculations, the AR concentration may be approximately regarded as constant. Thus, the kinetic equation at a constant pH can be simplified as follows:

$$-dC(t)/dt = kC(t), \quad (4)$$

where $C(t)$ is the current Fe(III) concentration in the reaction medium at the moment t ($t = 0$ corresponds to the moment of mixing the reagents), and k is the effective pseudo first order rate constant with respect to the Fe(III) concentration (the minus sign evidently corresponds to the decreasing Fe(III) concentration in the course of the reaction). Note that in Eq. (4), the concentration may be expressed in various units. For simplicity, we used $C(t)$ as a ratio between a current Fe(III) concentration and its initial concentration; so, at $t = 0$, $C(t) = 1$; thus, formally, $1 \geq C(t) \geq 0$.

Integration of Eq. (4) with the boundary conditions from $C(t) = 1$ to $C(t)$ and correspondingly from $t = 0$ to t gives the following simple expression:

$$\ln[C(t)] = -kt. \quad (5)$$

According to Eq. (5), the logarithm of the Fe(III) concentration (decreasing with time in the course of the redox process) should be directly proportional to the reaction time. Our experimental data (obtained from Mössbauer measurements; see Table 1) for the solutions of 5-MR, shown in a semilogarithmic plot, indeed show a very good linear correlation ($R^2 = 0.9993$); however, the line does not come out of the origin of coordinates (Fig. 4a; time t is given in min for clarity). The existing small intercept can logically be explained by the fact that, in the very initial moments of the reaction (a relatively short initial period), the freshly formed Fe(III) hydroxylated species may still undergo rapid ageing (which is typical for many freshly formed metal hydroxides), and thus be more reactive.

In this case, the kinetic Scheme (4) can be valid starting not from $t = 0$, but rather from some $t = t_1$ (where $t_1 > 0$), and so the relationship (4) becomes valid from $C(t_1) = C_1$.

Correspondingly, integration of Eq. (4) (after separating the variables) should be done for the boundary conditions from C_1 to $C(t)$, where $C(t) < C_1$, and from t_1 to t (where $t > t_1$), which finally gives the following expression (in decimal logarithms):

$$\log[C(t)] = (\log C_1 + 0.4343kt_1) - 0.4343kt. \quad (6)$$

Equation (6) reflects the existence of a small intercept, $(\log C_1 + 0.4343kt_1) = \text{const}$, in the linear dependence (see Fig. 4a). (Evidently, the k value can be calculated from the slope of the linear regression, whereas C_1 and t_1 cannot be simultaneously calculated from the intercept.) It may also be reasoned that, while $\log C_1$ is negative ($C_1 < 1$) and $0.4343kt_1$ is evidently positive, the overall value of the intercept (which is negative in both cases; see Fig. 4a, b) may be determined by the dominating $\log C_1$ value, especially for low k values (see below), such as in Fig. 4a, with t_1 expected to be of the order of up to ~1 min). However, C_1 and t_1 values may slightly differ in aqueous solution (Fig. 4a) and in the presence of 20 vol.% ethanol (Fig. 4b), which, along with different k values (see below), may account for a slight difference in the intercepts calculated according to Eq. (6): $\log[C(t = 0)] = -0.028$ and -0.044, respectively.

For the system involving 5-MR, in accordance with Eq. (6), the data in Fig. 4a give the following rate constant for the redox process at pH ~ 3: $k = (1.20 \pm 0.02) \times 10^{-5}$ s^{-1}. Our estimation for 4-*n*-HR (see Fig. 4b) gives $k = 9.1 \times 10^{-4}$ s^{-1} (i.e. virtually two orders of magnitude larger than that for 5-MR). Considering the same expected intercept value (dominated by the $\log C_1$ member at low k values, see above and Eq. (6)) for similar aqueous solutions of 5-MR (see Fig. 4a) and 5-*n*-PR, the redox rate constant for

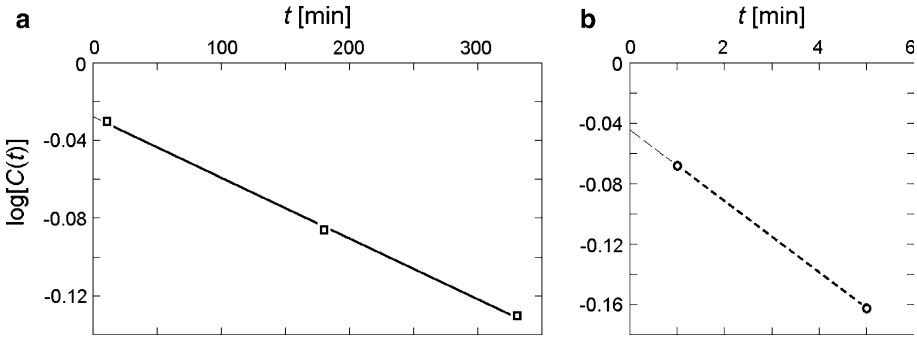

Fig. 4 Kinetics of iron(III) oxidation at pH ~ 3 by 5-methylresorcinol (**a**) and 4-*n*-hexylresorcinol (**b**). $C(t)$ represents the iron(III) concentration (in fractions of unity relative to the total iron concentration in solutions) calculated from Mössbauer spectroscopic data (see Table 1)

Table 2 Calculated values of the adiabatic ionisation potential (in eV) for resorcinol (1,3-dihydroxybenzene) and some of its alkylated derivatives

Substances	IP_{id}	IP_{zero}	IP_{therm}	IP_{Gibbs}
Resorcinol	7.98	7.99	7.98	7.97
5-Methylresorcinol	7.83	7.84	7.83	7.82
5-*n*-Propylresorcinol	7.73	7.74	7.74	7.75
4-*n*-Hexylresorcinol	7.52	7.55	7.54	7.57

Calculated from the difference of the total energy values between the cation radical and the initial molecule without (IP_{id}) and with the account of the zero-point vibrational energy (IP_{zero}), with the account of the zero-point vibrational energy and thermal corrections (IP_{therm}), from the difference of the Gibbs free energy values with the account of the zero-point vibrational energy and thermal energy (IP_{Gibbs})

the latter (see the data of Fig. 3e; Table 1) can be estimated as $k = 2.3 \times 10^{-6}\ s^{-1}$, i.e. yet fivefold lower than for 5-MR. Thus, the kinetic order of reaction rates from the experimental data (under the conditions applied in this study) is: 4-*n*-HR ($k = 9.1 \times 10^{-4}\ s^{-1}$) $\gg$ 5-MR ($k = 1.2 \times 10^{-5}\ s^{-1}$) $>$ 5-*n*-PR ($k = 2.3 \times 10^{-6}\ s^{-1}$).

DFT computational results

The thermodynamic measure of the ability of a molecule to donate an electron (i.e. to be oxidised) is the ionisation energy, which is commonly known as the ionisation potential (IP). The adiabatic IP ($IP_{adiabat}$) is determined by the difference between the minima of the potential surfaces for the cation radical (ionisation product) and for the initial molecule [46]. In this work, the $IP_{adiabat}$ values for non-alkylated *m*-dihydroxybenzene (resorcinol) and its three alkylated derivatives under study were calculated from the difference of the total energy values without (IP_{id}) and with the account of the zero-point vibrational energy (IP_{zero}); with the account of the zero-point vibrational energy and thermal corrections (IP_{therm}), as well as from the difference of the Gibbs free energy values with the account of the zero-point vibrational energy and thermal energy (IP_{Gibbs}). The results obtained are listed in Table 2.

As follows from Table 2, the differences between the calculated IP_{id}, IP_{zero}, IP_{therm} and IP_{Gibbs} values for each substance are within 0.02–0.05 eV. For comparison, the $IP_{adiabat}$ value experimentally measured by means of the photoionisation method for the structurally similar molecule, hydroquinone (*p*-dihydroxybenzene), was found to be 7.95 ± 0.03 eV [47]. Our computation results are also in good agreement with the data reported in [48], where the $IP_{adiabat}$ values for isolated (in vacuo) hydroquinone (7.96 eV), catechol (*o*-dihydroxybenzene; 8.19 eV) and resorcinol (8.23 eV) were calculated within the G3 theory by a methodology similar to that used in this work as the difference between the Gibbs free energy values for the cation radical and the initial molecule. Thus, the B3LYP/6-311++G(3*d*,3*p*) level is evidently sufficient for comparative evaluations of $IP_{adiabat}$ values in the series of resorcinol derivatives.

In accordance with any of the criteria (IP_{id}, IP_{zero}, IP_{therm} or IP_{Gibbs}; see Table 2), the ability to undergo oxidation should decrease in the following series:

4-*n*-Hexylresorcinol $\gg$ 5-*n*-propylresorcinol $>$ 5-methylresorcinol $\gg$ resorcinol.

Thus, the thermodynamic considerations predict that alkylation of resorcinol and further increasing the length of the alkyl substituent would enhance the reducing power of alkylated resorcinols.

Considering our experimental data (see above, Fig. 3; Table 1) as well as the reported inability of the non-alkylated analogue (resorcinol) to get oxidised under similar conditions [7], the corresponding experimental series is:

4-*n*-Hexylresorcinol $\gg$ 5-methylresorcinol $>$ 5-*n*-propylresorcinol $\gg$ resorcinol.

Thus, quantum chemical evaluations of $IP_{adiabat}$ in the series of these resorcinol derivatives, in line with experimental data, confirm the highest ability of 4-*n*-HR to donate electron in redox processes and the lowest ability to get oxidised for resorcinol [7]. However, thermodynamic considerations ($IP_{adiabat}$) predict a higher ability to be oxidised for 5-*n*-PR as compared with 5-MR, while experiment shows the opposite. This can probably be

ascribed to the effects of kinetic parameters (essential in aqueous media) related to, e.g. a higher hydrophobicity of the 5-*n*-PR and/or its expected lower diffusion coefficient (as compared to those for the 5-methyl derivative). As for the highest redox rate for the 4-*n*-hexyl derivative both found experimentally and predicted by DFT calculations, it may therefore be concluded that alkylation of resorcinol (1,3-dihydroxybenzene) in position 4 of the aromatic ring may be additionally favourable for oxidation of the resulting 4-ARs, as compared to 5-ARs, even for a longer 4-*n*-alkyl substituent.

The possibility of ARs to be oxidised by Fe(III) in weakly acidic media observed experimentally and confirmed by DFT calculations can be of ecological importance for the processes of microbial signalling in acidic soils and aquifers.

Conclusions

According to the experimental data obtained, 5-MR, 5-*n*-PR and 4-*n*-HR can be gradually oxidised by Fe(III) in weakly acidic aqueous media. However, their oxidation rates are strongly influenced by their molecular structure. The following series of the reduction rates were established: 4-*n*-HR $\gg$ 5-MR $>$ 5-*n*-PR $\gg$ resorcinol. The results obtained can have important implications for microbial ecology involving signalling processes in acidic environments.

Acknowledgments This work was supported in part under the Agreement on Scientific Cooperation between the Russian and Hungarian Academies of Sciences for 2011–2013 (Project 28), as well as under the European Research Area (ERA) Chemistry Programme (Project MCI-EUI 2009-04156; OTKA NN-84307).

Conflict of interest The authors declare that they have no conflict of interest.

References

1. Stevens AM, Schuster M, Rumbaugh KP (2012) Working together for the common good: cell–cell communication in bacteria. J Bacteriol 194:2131–2141
2. Stacy AR, Diggle SP, Whileley M (2012) Rules of engagement: defining bacterial communication. Curr Opin Microbiol 15: 155–161
3. Mangwani N, Dash HR, Chauhan A, Das S (2012) Bacterial quorum sensing: functional features and potential applications in biotechnology. J Mol Microbiol Biotechnol 22:215–227
4. Hense BA, Kuttler C, Müller J, Rothballer M, Hartmann A, Kreft J-U (2007) Does efficiency sensing unify diffusion and quorum sensing? Nat Rev Microbiol 5:230–239
5. Yates EA, Philipp B, Buckley C, Atkinson S, Chhabra SR, Sockett RE, Goldner M, Dessaux Y, Cámara M, Smith H, Williams P (2002) *N*-acylhomoserine lactones undergo lactonolysis in a pH-, temperature-, and acyl chain length-dependent manner during growth of *Yersinia pseudotuberculosis* and *Pseudomonas aeruginosa*. Infect Immun 70:5635–5646
6. Kamnev AA (2008) Chapter 13: Metals in soil versus plant–microbe interactions: biotic and chemical interferences. In: Barka EA, Clement C (eds) Plant–microbe interactions. Research Signpost, Trivandrum, pp 291–318
7. Pracht J, Boenigk J, Isenbeck-Schröter M, Keppler F, Schöler HF (2001) Abiotic Fe(III) induced mineralization of phenolic substances. Chemosphere 44:613–619
8. Kamnev AA, Kuzmann E (1997) Mössbauer spectroscopic evidence for the reduction of iron(III) by anthranilic acid in aqueous solution. Polyhedron 16:3353–3356
9. Kamnev AA, Kuzmann E (1997) Mössbauer spectroscopic study of the interaction of indole-3-acetic acid with iron(III) in aqueous solution. Biochem Mol Biol Int 41:575–581
10. Kovács K, Kamnev AA, Mink J, Németh Cs, Kuzmann E, Megyes T, Grósz T, Medzihradszky-Schweiger H, Vértes A (2006) Mössbauer, vibrational spectroscopic and solution X-ray diffraction studies of the structure of iron(III) complexes formed with indole-3-alkanoic acids in acidic aqueous solutions. Struct Chem 17:105–120
11. Kovács K, Sharma VK, Kamnev AA, Kuzmann E, Homonnay Z, Vértes A (2008) Water and time dependent interaction of iron(III) with indole-3-acetic acid. Struct Chem 19:109–114
12. Kamnev AA, Kovács K, Kuzmann E, Vértes A (2009) Application of Mössbauer spectroscopy for studying chemical effects of environmental factors on microbial signalling: redox processes involving iron(III) and some microbial autoinducer molecules. J Mol Struct 924–926:131–137
13. Von Uexkull HR, Mutert E (1995) Global extent, development and economic impact of acid soils. Plant Soil 171:1–15
14. Johnson DB, Kanao T, Hedrich S (2012) Redox transformations of iron at extremely low pH: fundamental and applied aspects. Front Microbiol 3:96. doi:10.3389/fmicb.2012.00096
15. Bolan NS, Hedley MJ, White RE (1991) Processes of soil acidification during nitrogen cycling with emphasis on legume based pastures. Plant Soil 134:53–63
16. Uroz S, Calvaruso C, Turpault R-P, Frey-Klett P (2009) Mineral weathering by bacteria: ecology, actors and mechanisms. Trends Microbiol 17(8):378–387
17. Chapman PJ, Ribbons DW (1976) Metabolism of resorcinylic compounds by bacteria: orcinol pathway in *Pseudomonas putida*. J Bacteriol 125:975–984
18. Kozubek A, Tyman JHP (1999) Resorcinolic lipids, the natural non-isoprenoid phenolic amphiphiles and their biological activity. Chem Rev 99:1–25
19. Stasiuk M, Kozubek A (2010) Biological activity of phenolic lipids. Cell Mol Life Sci 67:841–860
20. Sampietro DA, Belizán MME, Apud GR, Juarez JH, Vattuone MA, Catalán CAN (2013) Chapter 10: Alkylresorcinols: chemical properties, methods of analysis and potential uses in food, industry and plant protection. In: Céspedes CL, Sampietro DA, Seigler DS, Rai M (eds) Natural antioxidants and biocides from wild medicinal plants. CAB International, Wallingford, pp 148–166
21. Mulyukin AL, Filippova SN, Kozlova AN, Surgucheva NA, Bogdanova TI, Tsaplina IA, El'-Registan GI (2006) Non-species-specific effects of unacylated homoserine lactone and hexylresorcinol, low molecular weight autoregulators, on the growth and development of bacteria. Microbiology (Mosc) (Engl Transl) 75:405–414
22. Nikolaev YuA, Mulyukin AL, Stepanenko IYu, El'-Registan GI (2006) Autoregulation of stress response in microorganisms. Microbiology (Mosc) (Engl Transl) 75:420–426

23. El'-Registan GI, Mulyukin AL, Nikolaev YuA, Suzina NE, Gal'chenko VF, Duda VI (2006) Adaptogenic functions of extracellular autoregulators of microorganisms. Microbiology (Moscow) (Engl Transl) 75:380–389
24. Revina AA, Larionov OG, Kochetova MV, Lutsik TK, El'-Registan GI (2003) Spectrophotometric and chromatographic study of radiolysis products of aerated aqueous solutions of alkylresorcinols. Russ Chem Bull 52:2386–2392
25. Vértes A, Nagy D (eds) (1990) Mössbauer spectroscopy of frozen solutions. Akad. Kiadó, Budapest. Russian edition (Perfiliev YuD, translation editor). Mir, Moscow (1998)
26. Krebs C, Price JC, Baldwin J, Saleh L, Green MT, Bollinger JM Jr (2005) Rapid freeze-quench ^{57}Fe Mössbauer spectroscopy: monitoring changes of an iron-containing active site during a biochemical reaction. Inorg Chem 44:742–757
27. Krebs C, Bollinger JM Jr (2009) Freeze-quench ^{57}Fe Mössbauer spectroscopy: trapping reactive intermediates. Photosynth Res 102:295–304
28. Lam SW, Chiang K, Lim TM, Amal R, Low GK-C (2005) The role of ferric ion in the photochemical and photocatalytic oxidation of resorcinol. J Catal 234:292–299
29. Klencsár Z, Kuzmann E, Vértes A (1996) User-friendly software for Mössbauer spectrum analysis. J Radioanal Nucl Chem Articles 210:105–118
30. Kohn W (1999) Nobel Lecture: electronic structure of matter—wave functions and density functionals. Rev Mod Phys 71: 1253–1266
31. Koch W, Holthausen MC (2001) A chemist's guide to density functional theory. Wiley-VCH, Toronto
32. Sousa SF, Fernandes PA, Ramos MJ (2007) General performance of density functionals. J Phys Chem A 111:10439–10452. doi:10.1021/jp0734474
33. Becke AD (1988) Density-functional exchange-energy approximation with correct asymptotic behavior. Phys Rev A 38: 3098–3100
34. Becke AD (1993) Density-functional thermochemistry. III. The role of exact exchange. J Chem Phys 98:5648–5652
35. Lee C, Yang W, Parr RG (1988) Development of the Colle–Salvetti correlation-energy formula into a functional of the electron density. Phys Rev B 37:785–789
36. Krishnan R, Binkley JS, Seeger R, Pople JA (1980) Self-consistent molecular orbital methods. XX. A basis set for correlated wave functions. J Chem Phys 72:650–654
37. McLean AD, Chandler GS (1980) Contracted Gaussian basis sets for molecular calculations. I. Second row atoms, Z = 11–18. J Chem Phys 72:5639–5648
38. Frisch MJ, Trucks GW, Schlegel HB, Scuseria GE, Robb MA, Cheeseman JR, Zakrzewski VG, Montgomery JA, Stratmann RE, Burant JC, Dapprich S, Millan JM, Daniels AD, Kudin KN, Strain MC, Farkas O, Tomasi J, Barone V, Cossi M, Cammi R, Mennucci B, Pomelli C, Adamo C, Clifford S, Ochterski J, Petersson GA, Ayala PY, Cui Q, Morokuma K, Malick DK, Rabuck AD, Raghavachari K, Foresman JB, Cioslowski J, Ortiz JV, Baboul AG, Stefanov BB, Liu G, Liashenko A, Piskorz P, Komaromi I, Gomperts R, Martin RL, Fox DJ, Keith T, Al-Laham MA, Peng CY, Nanayakkara A, Gonzales C, Challacombe M, Gill PMW, Johnson B, Chen W, Wong MW, Andreas JL, Head-Gordon M, Reploge ES, Pople JA (2003) Gaussian 03, revision B.03. Gaussian, Inc., Pittsburgh
39. Pankratov AN (2007) Electronic structure and reactivity of inorganic, organic, organoelement and coordination compounds: an experience in the area of applied quantum chemistry. In: Kaisas MP (ed) Quantum chemistry research trends. Nova Science Publishers, Inc., New York, pp 57–125
40. Froimowitz M (1993) HyperChem: a software package for computational chemistry and molecular modeling. Biotechniques 14:1010–1013
41. Stewart JJP (1989) Optimization of parameters for semiempirical methods. I. Method. J Comput Chem 10:209–220
42. Stewart JJP (1989) Optimization of parameters for semiempirical methods. II. Applications. J Comput Chem 10:221–264
43. Gütlich P, Bill E, Trautwein A (2011) Mössbauer spectroscopy and transition metal chemistry. Springer, Berlin
44. Kuzmann E, Homonnay Z, Nagy S, Nomura K (2010) Mössbauer spectroscopy. In: Vértes A, Nagy S, Klencsár Z (eds) Handbook of nuclear chemistry, vol 2., Elements and isotopes: formation, transformation, distribution. Springer, Dordrecht, pp 3–65
45. Singh US, Scannell RT, An H, Carter BJ, Hecht SM (1995) DNA cleavage by di- and trihydroxyalkylbenzenes. Characterization of products and the roles of O_2, Cu(II), and alkali. J Am Chem Soc 117:12691–12699
46. Dykstra CE, Frenking G, Kim KS, Scuseria GE (2011) Theory and applications of computational chemistry: the first forty years. Elsevier, Amsterdam, 1308 pp
47. Gurvich LV, Karachevtsev GV, Kondratyev VN, Lebedev YuA, Medvedev VA, Potapov VK, Khodeev YuS (1974) Energii razryva khimicheskikh svyazei. Potentsialy ionizatsii i srodstvo k elektronu („Energies of disruption of chemical bonds. Ionisation potentials and affinity to the electron", in Russ.). Nauka, Moscow, 351 pp
48. Canevari TC, Arenas LT, Landers R, Custodio R, Gushikem Y (2013) Simultaneous electroanalytical determination of hydroquinone and catechol in the presence of resorcinol at an SiO_2/C electrode spin-coated with a thin film of Nb_2O_5. Analyst 138:315–324